LLC Resonant DC-DC Converter for High Efficiency Solar Array Simulator

Smita Agrawal
Student (Power Electronics),
Department of EEE,
The Oxford College of Engineering,
Bangalore.

***Abstract*— In this paper a LLC resonant DC-DC converter is proposed for a high a high efficiency solar array simulator(SAS).this circuit saves the cost of photovoltaic system testing. In this proposed converter circuit primary switches has ZVS operation and rectifier diodes has ZCS operation . With the use of frequency modulation control, circuit impedance can be regulated from zero to infinite without use of shunt or serial resistors, in this way efficiency is increased of the proposed SAS. The circuit operation and its different mode of operation are analyzed and circuit parameters are designed considering practical consideration.**

Index Terms*—:- SAS, PV system, LLC resonant DC-DC converter.

I. INTRODUCTION

Traditional energy resources are limited and can be exhausted in the near future. Therefore, developing renewable energy resources to replace existing traditional energy resource is necessary. There are many forms of renewable energy resources among them solar power is most attractive because vast amounts of energy is freely available, and it is noiseless and pollution-free. A solar array is subjected to large temperature changes and changes in insolation because atmospheric conditions are uncontrollable. In order to test the solar array power environment, a cost-effective solution is to utilize a solar array simulator. A solar array simulator provides illumination which is an approximation of natural sunlight. Solar array simulator provides controllable indoor test facility under lab conditions for testing of solar cells. In early days of solar power metal-halide lamps and temperature controlling devices was used to test the illumination and temperature of PV arrays. But the cost of temperature controlling devices high and the metal-halide lamps consumes large amount of power resulting additional energy waste. Therefore, the literatures proposed solar array simulators (SASs) which is used to provide PV characteristics directly. There are various types of solar array simulators. One approach for high-power systems is pulse width modulation dc–dc converters used to generate PV characteristics. But shunt resistors are used to limit output voltage and serial resistors are required to inhibit spike current at high duty-ratio and at low duty-ratio operation respectively. These shunt and serial resistors causes additional power dissipations and thereby affects efficiency. In addition to that, power switches of PWM converter operates in hard switching resulting high switching losses and electromagnetic interference. in case of resonant converters , the output impedance can be regulated from zero to infinite by using method of frequency modulation control.in resonant converters shunt and serial resistors are not used therefore this approach resonant is more suitable than the PWM dc–dc converters for the solar array simulator applications. There are various types of resonant converters among them satisfied efficiency can be achieved with series resonant converter (SRC) but at light load condition problem of output voltage regulation is there. In case of parallel resonant converter (PRC) there is no light load regulation issue but its circulating energy is much higher than in case of series resonant converter and affects its efficiency significantly . Series-parallel resonant converter (SPRC) has the advantages of SRC and PRC. It has smaller circulating energy and it is not so sensitive to load change. But same as in case of SRC and PRC, high switching frequency operation is required in SPRC to get very low output-voltage. Therefore, all SRC, PRC, and SPRC possess high circulating energy at low output-voltage operation and thereby lower their Efficiencies. This paper proposes a high-efficiency SAS implemented by an LLC resonant dc–dc converter. The LLC resonant converter has smaller circulating energy than SRC, PRC, and SPRC in case of high input-voltage or low output-voltage operation. converter switches can turn ON with zero-voltage switching (ZVS), and output rectifier diodes can turn OFF with zero-current switching (ZCS), resulting higher conversion efficiency. With frequency modulation control, LLC converter output impedance can be regulated without use of shunt or serial resistors from zero to infinite; therefore, efficiency of the proposed Is significantly increased. For electrical isolation Converter has a transformer to provide electrical isolation. In this paper, the theoretical equations and operation principles and Circuit parameters are designed based on the practical considerations.

II. CHARACTERISTICS OF SOLAR CELLS

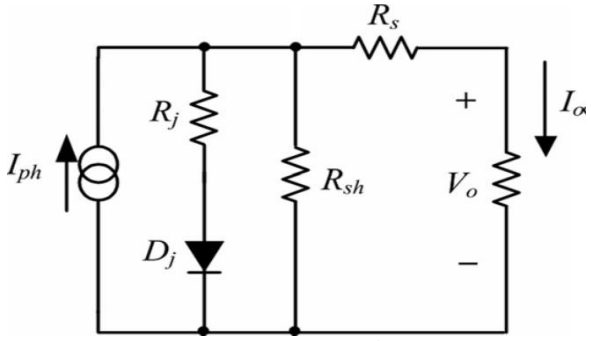

Fig1. Equivalent circuit of a solar cell.

Solar cells are p–n junction semiconductor which is used to transform solar energy into electricity. Fig.1 is showing an equivalent circuit of a solar cell. In fig.1 R_{sh} and R_s are intrinsic shunt and serial resistors of the cell, respectively. The current source I_{ph} represents the cell photocurrent, which is a function of illumination Si and solar array temperature T, and can be expressed as follows:

$$Iph = \frac{[ISSO + Ki(T - Tr)]Si}{100}$$

Where I_{sso} is the short-circuit current at reference temperature Tr and reference illumination (100 mW/cm2), and Ki is temperature coefficient of the short-circuit current. Additionally, D_j expresses the p–n junction of a solar cell, and R_j is its nonlinear resistance. I_{sat} represents the reversed saturation current of D_j and can be expressed as follows:

$$Isat = Irr\left[\frac{T}{Tr}\right]^3 exp\left[\frac{qEG}{kA}\left(\frac{1}{Tr} - \frac{1}{T}\right)\right]$$

Where I_{rr} is the corresponding reversed saturation current at T_r, E_{Gap} is the band-gap energy of the semiconductor used in the cell, q is charge of an electron (1.6 ×10−19 C), k is Boltzmann's constant (1.38 × 10−23 J/K), and A is the ideality factor of the p–n junction. If there are n_s cells connected in series and n_p cells connected in parallel, the output characteristic of PV arrays can be represented by the following equations:

$$I0 = np\,Iph - npIsat\left[exp\left(\frac{q}{kTA}\,\frac{V0 - I0Rs}{ns}\right) - 1\right] - \frac{V0 - I0Rs}{Rsh}$$

$P_0=V_0I_0$

III. ANALYSIS OF THE LLC RESONANT DC–DC CONVERTER

Fig. 2 shows the circuit diagram of an LLC resonant dc–dc converter consisting an LLC resonant inverter, a current-driven transformer with a center-tapped rectifier. LLC converter is similar to that of SRC with the main difference, the magnetizing inductance Lm is slightly higher than the resonant inductance Lr in the LLC converter .at some load conditions, Lm participate in the resonance with Lr and Cr and change the characteristics of resonant tank.

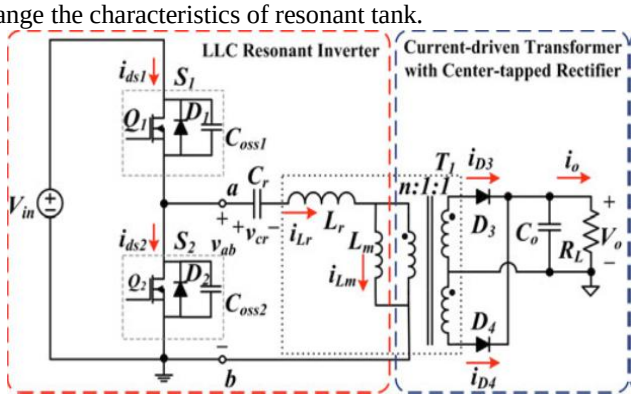

Fig. 2. Circuit diagram of LLC resonant dc/dc converter.

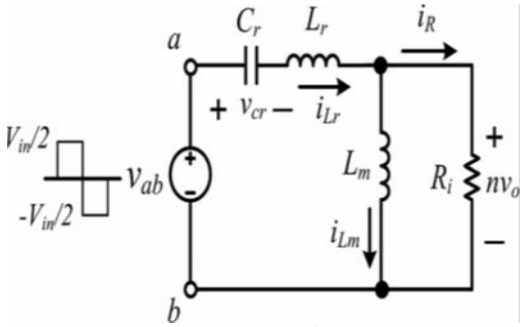

Fig. 3. Equivalent circuit of the LLC resonant converter

Fig. 3 shows the equivalent circuit of the LLC resonant inverter in which Ri is equivalent load resistance seen in primary side and can be expressed as Ri =8n2RL /π2 .

$$|M_V(\omega)| = \left|\frac{V_o}{V_{in}}\right| = \frac{1}{2n\left\{\sqrt{(1+A)^2[1-(\omega_L/\omega)^2]^2 + \left(1/Q_L\right)^2\left((\omega_L/\omega)\left(A/(1+A)\right) - (\omega_L/\omega)\right)^2}\right\}}$$

$$A = \frac{L_r}{L_m}$$

$$\omega_L = 2\pi f_L = \frac{1}{\sqrt{(L_r + L_m).C_r}}$$

$$Q_L = R_i \times \sqrt{\frac{C_r}{L_r + L_m}} = R_i.\omega_L.C_r$$

$$\omega_h = 2\pi f_H = \frac{1}{\sqrt{L_r.C_r}}$$

Fig. 4 shows the frequency response of the LLC resonant converter. Two resonant frequencies are there. ωL is second resonant frequency and ωH is the main resonant frequency . According to the resonant frequencies of ωH and ωL Fig. 4 can be divided into three operation regions. Impedance of resonant tank is capacitive in Region 3, therefore the primary switches can operate under ZCS condition. But the current spike during turn-on transient will result in high-current stress and high-switching loss. Therefore, LLC resonant converters should not operate in this region.

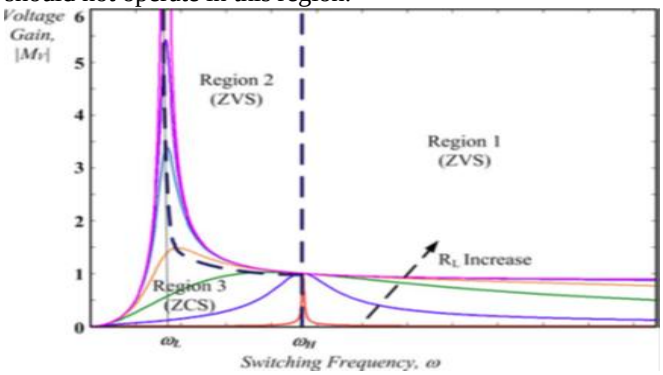

Fig. 4. Frequency response of output voltage gain of the LLC resonant converter.

In region 1 impedance of resonant tank is inductive therefore switches can operate under ZVS condition to reduce switching loss. But secondary rectifier diodes cannot operate under ZCS. Voltage spikes during turn-off transient results in high switching loss.

In region 2, the switching frequency is lower than the main resonant frequency ω_H , the converter is of boost type. During main resonant period, voltage of Lm is clamped by output voltage and the inductor current i_{Lm} is linearly increasing. When i_{Lm} reaches the same level as the resonant current i_{Lr} , a second resonance occurs. This resonance continues until the primary switches switching again so that the converter can still operate under ZVS. Besides, during the second resonant period, the current of secondary rectifier diodes remains zero; hence, they can turn OFF naturally under ZCS condition.

For practical considerations, minimizing power dissipation of SAS and preventing the operation entering region 3, the switching frequency of SAS operating in maximum output power is designed slightly higher than resonant frequency ω_L.

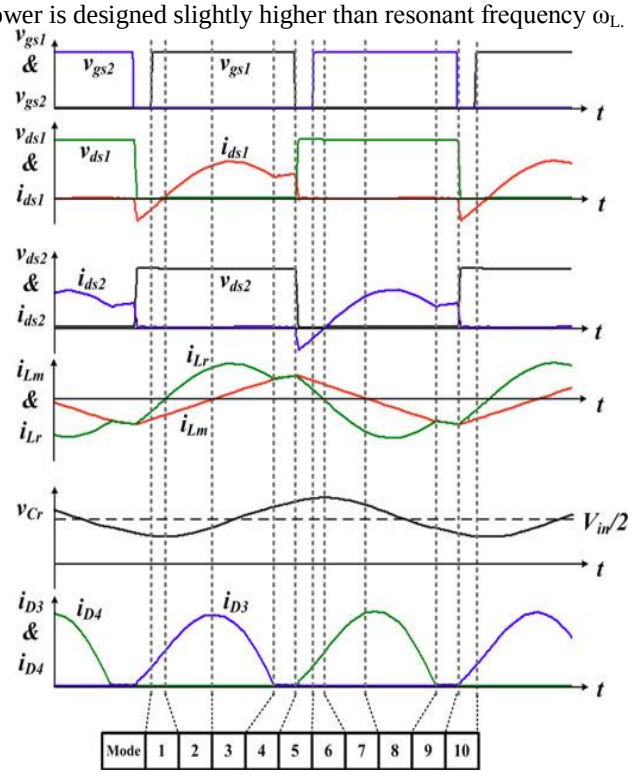

Fig. 5. Main waveforms of the LLC resonant converter operating in region 2.

IV. IV. OPERATION PRINCIPLES OF THE LLC RESONANT DC–DC CONVERTER

As shown in Fig. 2, the primary switches S1 (S2) are composed of an MOSFET Q1 (Q2), and its intrinsic antiparallel diode D1 (D2) and equivalent output capacitor COSS1 (COSS2). The resonant tank is formed by the resonant capacitor Cr , and the leakage inductor Lr and magnetizing inductor Lm of the transformer T1 . The center-tapped rectifier is constructed by connecting diodes D3 and D4 to the secondary windings of T1 .

Based on the analysis of earlier section, the main theoretical waveforms of the LLC resonant converter operating in region 2 are shown in Fig. 5. There are ten operation modes within one switching period. Because the waveforms are symmetrical, only the operation principles of the first five modes are introduced referring to the equivalent circuits shown in Fig. 6.

A. Mode 1

This mode starts when the switch S1 is turned ON under ZVS. The equivalent circuit is shown in Fig. 6(a). The resonant current i_{Lr} is sine-wave and increases from negative to discharge Cr , and energy returns to the input voltage source. The voltage of L_m is clamped to nV_O so that the magnetizing current i_{Lm} increases linearly from negative. The energy stored in L_m will be released through D3 to output load. When i_{Lr} reaches zero, this mode ends.

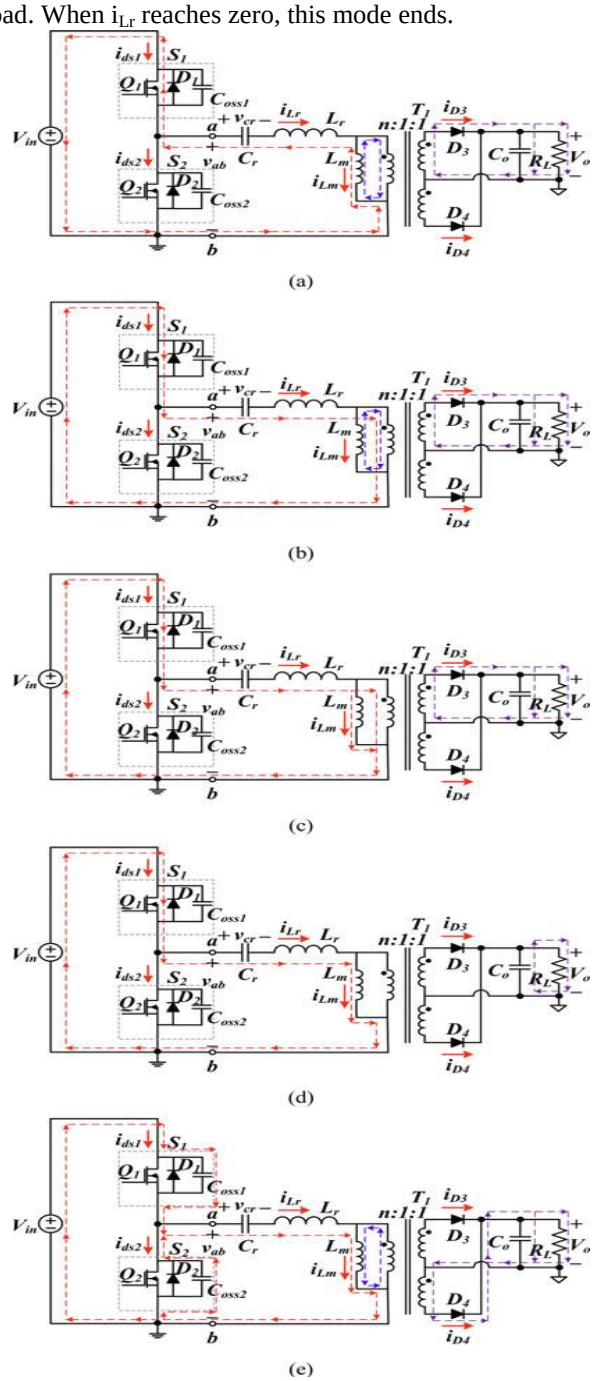

Fig. 6. Equivalent circuits of (a) Mode 1, (b) Mode 2, (c) Mode 3, (d) Mode4, and (e) Mode 5 for the LLC converter operating in region 2.

B. Mode 2

As shown in Fig. 6(b), since i_{Lr} increases from zero to positive, the input voltage source charges Cr and L_r , and supplies energy to output load simultaneously. The energy in Lm is released to output load continuously. When i_{Lm} reaches zero, this mode ends.

C. Mode 3

At this mode, because the voltage of Lm is still clamped to nV_O, i_{Lm} remains increasing linearly. The input voltage source charges Lm and supplies energy to output load. The equivalent circuit is shown in Fig. 6(c).

D. Mode 4

This mode starts when i_{Lr} and i_{Lm} equal each other. Current circulating through the secondary diode D3 naturally decreases to zero so that this diode turns OFF under ZCS condition. The voltage spike caused by diode reverse recovery would not exist. The voltage of Lm is no longer clamped to nV_O , hence, Lm is in series with L_r and participates in the resonance with Cr. The equivalent circuit of this mode is shown in Fig. 6(d). Because the equivalent inductance of (Lr + Lm) is higher than L_r, as shown in Fig. 5, i_{Lr} and i_{Lm} are almost constant in this short time interval.

E. Mode 5

As shown in Fig. 6(e), while S1 is turning OFF, the resonant current i_{Lr} is charging COSS1 and discharging COSS2 simultaneously. At the moment of vds2 decreasing to zero, the resonant current i_{Lr} flows through antiparalleled diode D2 which provide ZVS operation for S2 turn ON. At the same time, the secondary rectifier diode D4 turns ON. The voltage of Lm is clamped to nV_O with reverse polarity so that the current i_{Lm} becomes decreasing linearly. The magnetizing inductor Lm is separated from the resonance with Cr .When S2 turns ON under ZVS, this mode ends and enters the half cycle with symmetrical operation principles.

V. DESIGN SPECIFICATIONS AND CONSIDERATIONS

To verify the feasibility of the proposed SAS implemented by an LLC resonant converter, an illustrative example is built to provide the electrical characteristics of the PV module F-MSN- 75W-R-02 (Motech Company, Ltd.). Considering the normal operation temperature of 25 ◦C and the maximum illumination of 80 mW/cm2 , the electrical characteristics of F-MSN-75WR- 02 can be determined from (1) to (4) and shown in Table I. Hence, the output specifications of the SAS are defined as 59W, 0–21 V, and 0–4 A

Considering the problems of current harmonic distortions induced by rectifiers, the proposed SAS is designed to operate with an active power factor corrector in the front end. Therefore, its input voltage is set at 400 V_{dc}. The main resonant frequency f_H is determined at 100 kHz. The design considerations for component parameters are introduced as follows.

TABLE I
ELECTRICAL CHARACTERISTICS OF THE PV MODULE F-MSN-75W-R-02 AT 80 mW/cm2 AND 25 ◦C

F-MSN-75W-R-02 at 80mW/cm^2 and 25°C	
Maximum Power, P_{max}	59 W
Voltage of Maximum Power Point, V_{mpp}	18 V
Current of Maximum Power Point, I_{mpp}	3.3 A
Voltage of Open Circuit Point, V_{OC}	21 V
Current of Short Circuit Point, I_{SC}	4 A

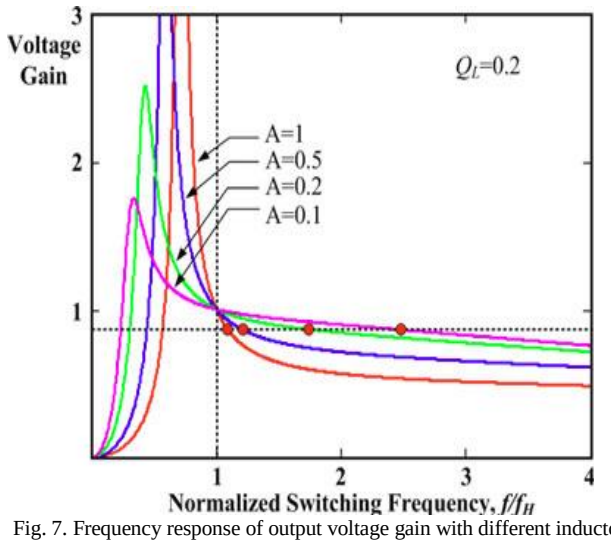

Fig. 7. Frequency response of output voltage gain with different inductor ratios.

A. Inductor Ratio (A = Lr / Lm)

Since the output voltage of the SAS is from 0 to 21 V, the LLC resonant converter should operate in both regions 1 and 2. According to (5), Fig. 7 shows the frequency response of voltage gain related to different inductor ratio. In region 1, if the inductor ratio is higher, the lower voltage gain can be easily obtained by increasing frequency slightly. However, high-inductor ratio results in sharp slope of voltage gain in region 2, which might impact the stability of frequency modulation control. For tradeoff, the inductor ratio A is set at 0.5. Hence, the secondary resonant frequency fL can be calculated from (7) and (9) to be 57.7 kHz.

B. Turn Ratio of Transformer

Based on the previous analysis, the optimal efficiency of an LLC resonant converter is located in region 2. To ensure that the converter operates in region 2 at maximum power condition, we set switching frequency equal to the main resonant frequency (f = fH) when the output voltage Vo = 14 V. Considering duty ratio D = 0.5 and diode forward voltage VF = 0.7 V, the minimum turn ratio can be determined from

$$n \geq \frac{V_{in} \cdot D}{(V_o + V_F)} \cong 13.6$$

We select n = 14 in this design.

C. Components of Resonant Tank (Lm, Lr , and Cr)

The magnetizing inductor Lm should meet the condition expressed in (11) so that the primary switches can turn ON under ZVS

$$L_m \le \frac{nV_0T_s \cdot t_{d,min}}{8C_{oss} \cdot V_{in}}$$

The equivalent output capacitance of power MOSFETs Coss is 90 nF, and the minimum dead time td, min is 200 ns. Therefore, the maximum inductance of Lm can be expressed as follows:

$$L_{m,max} = \frac{nV_0T_s \cdot t_{d,min}}{8C_{oss} \cdot V_{in}} = 13.6\ mH$$

According to the definition of inductor ratio (A=Lr /Lm), the maximum inductance of Lr can also be determined as follows:

$$L_{r,max} = A \cdot L_{m,max} = 680.6\ \mu H$$

There are several standard capacitances to obtain the desired fL with 57.7 kHz. Cr is chosen as 3.9 nF in this case. Hence, Lr = 650 µH and Lm = 1.3 mH can be obtained from (7) and (9).

VI. SIMULATION RESULTS

Based on the previous design, the electrical specifications and component parameters of the LLC resonant converter are summarized in Table II.

TABLE II
ELECTRICAL SPECIFICATIONS AND COMPONENT PARAMETERS

Electrical Specifications	
Input Voltage, V_{in}	400V
Output Voltage, V_O	0 – 21V
Output Current, I_O	0 – 4A
Maximum Power, P_O	60W
Main Resonant Frequency, f_H	100 kHz
Secondary Resonant Frequency, f_L	57.7 kHz
Switching Frequency	60 – 250 kHz
Component Parameters	
Resonant Inductor, L_r	650 µH
Magnetizing Inductor, L_m	1.3 mH
Resonant Capacitor, C_r	3.9 nF
Transformer Turn Ratio, n:1:1	14:1:1
Primary Switch, S_1 and S_2	STP10NK60Z
Rectifier Diode, D_3 and D_4	STPS3045CW

Fig. 9 shows the simulation circuit. Fig. 10 shows the voltage and current waveforms of the primary switch S1 and S2, when the SAS operates at the maximum power point (MPP).

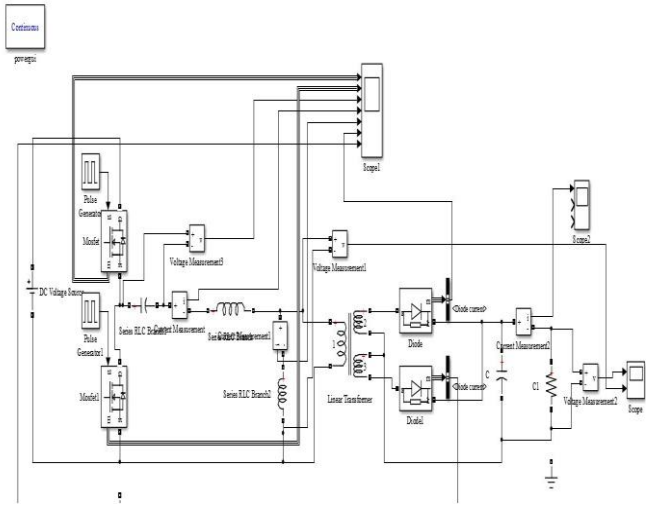

Fig. 9 simulation circuit of LLC resonant DC-DC converter implanted for high efficiency solar array simulator

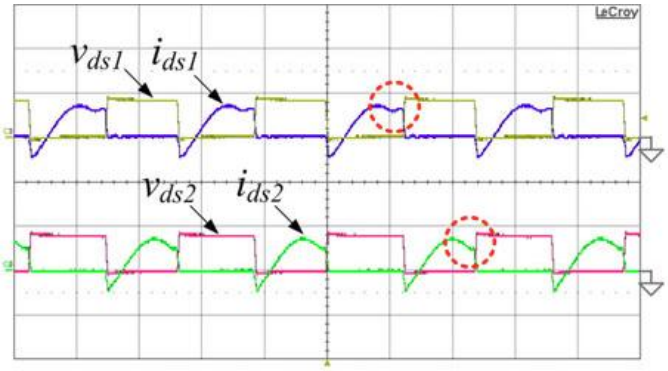

Fig. 10. Measured voltage and current waveforms of primary switches S1 and S2 when the proposed SAS operates at MPP

It could be observed that S1 and S2 can turn ON under ZVS condition. the turn-off current can be reduced by the second resonance, as shown in Fig. 10. Therefore, the circulating energy and turn-off loss can be significantly minimized to improve system efficiency.

VII. CONCLUSION

A high-efficiency SAS implemented by an LLC resonant converter with ZVS feature has been proposed. The detail operation principle, design procedures, and considerations are introduced.

VII. REFERENCES

1. N. Femia, G. Petrone, G. Spagnuolo, and M. Vitelli, "Optimization of perturb and observe maximum power point tracking method," IEEE Trans. Power Electron., vol. 20, no. 4, pp. 963–973, Jul. 2005.
2. A. K. Abdelsalam, A. M. Massoud, S. Ahmed, and P. N. Enjeti, "High-performance adaptive perturb and observe MPPT technique for photovoltaic-based microgrids," IEEE Trans. Power Electron., vol. 26, no. 4, pp. 1010–1021, Apr. 2011.
3. F.Nagamine, R. Shimokawa,M. Suzuki, and T. Abe, "Newsolar simulator formulti-junction solar cell measurements," in Proc.Conf. Rec. 23rd IEEE Photovoltaic Spec. Conf., May 1993, pp. 686–690.
4. S. Techajunta, S. Chirarattananon, and R. H. B. Exell, "Experiments in a solar simulator on solid desiccant regeneration and air dehumidification for air conditioning in a tropical humid climate," Renewable Energy, vol. 17, no. 4, pp. 549–568, Aug. 1999.
5. A. K.Mukerjee and N. Dasgupta, "DC power supply used as photovoltaic simulator for testing MPPT algorithms," Renewable Energy, vol. 32, no. 4, pp. 587–592, Apr. 2007.
6. L.A. C. Lopes and A.-M. Lienhardt, "A simplified nonlinear power source for simulating PV panels," in Proc. IEEE Power Electron. Spec. Conf., Jun. 2003, pp. 1729–1734.
7. H. Nagayoshi, "I-V curve simulation by multi-module simulator using I-V magnifier circuit," Solar Energy Mater. Solar Cells, vol. 82, no. 1–2,pp. 159–167, May 2004.